Flexible anodic SnO2 nanoporous structures uniformly coated with polyaniline as a binder-free anode for lithium ion batteries

Nahyun Shin, Moonsu Kim, Jaeyun Ha, Yong-Tae Kim, Jinsub Choi

Flexible anodic SnO₂ nanoporous structures uniformly coated with polyaniline as a binder-free anode for lithium ion batteries

Nahyun Shin [a], Moonsu Kim [a,b], Jaeyun Ha [a], Yong-Tae Kim [a,]*, Jinsub Choi [a,]*

[a] Department of Chemistry and Chemical Engineering

Inha University, 22212, Incheon, Republic of Korea

[b] Univ. Renns 1, CNRS, ISCR (Institut des Sciences Chimiques de Rennes)
-UMR6226, F-35000 Rennes, France

*To whom correspondence should be addressed.

Tel: +82-32-860-7476

e-mail: yongtaekim@inha.ac.kr, jinsub@inha.ac.kr

Abstract

Herein we report a wet-chemical process to obtain binder-free anodes for lithium-ion batteries (LIBs) using a straightforward and easily scalable approach. Electrochemical deposition, anodization, and electropolymerization are used to firmly attach a nanoporous and flexible SnO_2 film, uniformly coated with polyaniline (PANI), onto a Cu substrate. The three-dimensional, flexible, and nanoporous SnO_2@PANI electrodes exhibit good specific capacity, capacity retention, and charge transfer resistance. Its favorable electrochemical properties are attributed to the large surface area, high electrical conductivity, and effective reduction of volume expansion. These results demonstrate that the proposed approach to forming SnO_2@PANI electrodes is a promising strategy for constructing high-performance binder-free anodes for emerging flexible LIBs.

Keywords: SnO_2; polyaniline; volume expansion; lithium diffusion; lithium-ion batteries.

1. Introduction

There is a growing need to develop renewable energy technologies and effective energy storage systems to address environmental pollution and the energy crisis. Consequentially, there is an increased demand for stable lithium-ion batteries (LIBs) with high energy density and long lifespan that can be used in portable electronic devices, electric vehicles (EVs), and massive energy storage system (ESS).[1, 2] Although graphite is currently used in commercial LIBs, its low specific capacity (372 mA h g^{-1}) renders it ill-suited to meet the high energy and power density required by next-generation LIBs.[3] Among various anode materials that show promise as alternatives to graphite, SnO_2 is considered a possible candidate due to its ultrahigh theoretical specific capacity of 1494 mA h g^{-1} and low electrode potential compared with Li/Li$^+$ (0–1 V). In addition, SnO_2 is highly abundant, inexpensive, and environmentally benign.[4-7] However, the large volume expansion (300%) and low conductivity of SnO_2 cause several challenging issues relating to mechanical stress and pulverization of the electrode during lithiation; these critical drawbacks must be addressed before LIBs made with SnO_2 anodes can be commericialized.[8-10] There have been several attempts to reduce the volume expansion of SnO_2 and shorten the Li ion diffusion transport length through electrode micro-/nanoization and using a buffered matrix.[11-13]

Recently, self-aligned electrodes have been grown directly onto current collectors without using conductive additives or binders, and their ability to increase battery energy density and prevent electrochemical side reactions between binder and electrolyte has been investigated.[14-16] These studies have shown that anodization is a straightforward technique to grow layers of self-aligned metal oxide with varied structures onto valve metals like Al, Ti, etc.[17, 18] Anodic porous alumina is widely used as a template to prepare many functional materials for optical,

electronic, and electrochemical applications, and anodic tubular titania is used for gas-sensing or catalytic applications. SnO_2 nanostructures prepared by anodization can be similarly useful as favorable binder-free anode materials for LIBs owing to their improved capacity to accommodate volume expansion during lithiation. Furthermore, coating the SnO_2 electrode with a conductive polymer can efficiently suppress volume expansion and also improve electron transport by enhancing electrical conductivity.[19-21] In particular, polyaniline (PANI) as one of the nitrogen-rich conducting polymers, is excellent candidate due to its outstanding electrical conductivity from the conjugated p-electron system, good structural stability, flexibility, and ease of synthesis properties.[22, 23]

Herein, we demonstrate a simple and easily scalable approach for fabricating nanoporous polyaniline-coated SnO_2 (SnO_2@PANI) anodes for LIBs via electrochemical deposition of Sn onto a Cu substrate, anodization, and subsequent PANI electropolymerization. We employed the cost-effective and scalable approach (compared with conventional coating technology) of optimizing anodizing conditions and controlling electropolymerization to achieve nanoporous SnO_2@PANI electrodes with high surface areas, shorter Li ion diffusion lengths, low resistances, and effective reduction in volume expansion.

2. Experimental

2.1. Preparation of SnO$_2$ electrode on Cu foil

Prior to electrochemical deposition, Cu foil (0.127 mm thick, 99.9%, Alfa Aesar) was cut into dimensions of 1.5 cm × 1.5 cm and degreased in sequence with acetone, ethanol, and deionized (DI) water by ultrasonication for 10 min. The electrochemical deposition of Sn on the Cu substrate was performed using a two-electrode system composed of Cu foil and Pt mesh as the working and counter electrodes, respectively. A current density of 10 mA cm^{-2} was applied for 10 min in an aqueous electrolyte consisting of 0.22 M SnCl$_2$ and 0.31 M sodium citrate tribasic dihydrate. The anodization of Sn deposited onto the Cu foil substrate was carried out in a 0.1% oxalic acid electrolyte at different voltages and for different times. Anodized samples were subsequently rinsed with DI water and dried in an oven at 60 °C.

2.2. Preparation of SnO$_2$@PANI electrode

Electropolymerization of PANI onto the SnO$_2$ electrode was performed in an electrolyte composed of 0.2 M oxalic acid and 0.1 M aniline at 25 °C. A standard three-electrode cell of SnO$_2$ on Cu foil, Pt mesh, and Ag/AgCl were used as the working, counter, and reference electrodes, respectively. The SnO$_2$@PANI electrodes were obtained by applying a potential from −0.5 to 1.5 V (vs. Ag/AgCl) at different scan rates ranging from 60 to 120 mV s^{-1}. for three cycles. The obtained electrodes were rinsed with DI water and dried in an oven at 60 °C.

2.3. Material Characterization

The morphologies of the prepared electrodes were characterized using a field-emission scanning electron microscope (FE–SEM, S–4300, Hitachi, instrument at Core–Facility Center for Sustainable Energy Materials of Korea Basic Science Institute (KBSI)) and a field–

emission transmission electron microscope (FE–TEM; JEM–2100F, JEOL, Japan) equipped with an energy-dispersive X-ray spectrometer (EDS). The crystallinity of the samples was analyzed using an X-ray diffractometer (XRD; DMAX 2200V PC, Rigaku, Japan) with Cu Kα radiation (λ = 1.54056 Å). X-ray photoelectron spectroscopy (XPS, K–Alpha, Thermo Fisher Scientific, USA) was employed to determine the elemental binding states of the samples.

2.4. Electrochemical Characterization

The SnO_2@PANI electrodes as a binder-free electrode for LIBs were characterized using CR2032 coin-type half-cell, which was assembled in an Ar-filled glove box with less than 0.3 ppm O_2 and H_2O. The as-prepared samples had a diameter of 1 cm and were used as the working electrode, with pure Li foil used as the counter electrode. A glass fiber (GF/A, Whatman) with a diameter of 1.6 cm was used as the separator, and a 1 M solution of $LiPF_6$ dissolved in a 50:50 (w/w) mixture of ethylene carbonate (EC) and diethyl carbonate (DMC) was employed as the electrolyte. The galvanostatic charge and discharge cycling tests were performed in the potential range of 0.01–3.0 V (vs. Li/Li$^+$) using a battery test cycler (CT–4009T–5V50mA–164, Sinopro). Cyclic voltammetry (CV) measurements were conducted using an electrochemical workstation (SP–150, Bio–Logic, Seyssinet–Pariset, France) between 0.01 and 3 V at a scan rate of 0.1 mV s^{-1}. Electrochemical impedance spectroscopy (EIS) was performed using an electrochemical workstation (PGSTAT302N Autolab, Metrohm) in the frequency range from 100 kHz to 0.01 Hz with a voltage amplitude of 5 mV.

3. Results and Discussion

3.1. Material characterization

SnO$_2$@PANI electrodes are fabricated by electrochemical deposition, followed by anodization, and subsequent electropolymerization, as illustrated in Scheme 1. As shown in Figure S1, after a short transient response, the current density becomes stable, resulting in uniform deposition of Sn metal on the entire Cu foil substrate.[24] The surface structure of Sn is rough, primarily due to Sn (the condensed species) having a greater surface energy than the substrate (Cu foil), as explained by the Volmer–Weber growth model.[25] The current density vs. time transient plot recorded during anodization (Figure 1(a)) demonstrates that this process can be divided into three steps. In step I, the current density drops sharply owing to the formation of an oxide barrier layer. Within a few oscillations, the current density reaches a steady state (step II), indicating growth of a porous oxide structure composed of discontinuous nanochannels with thin gaps separating each layer (Figure 1(b), where the anodization was performed at 10 V for 15 min). The formation of these longitudinally discontinuous layers is attributed to vigorous oxygen evolution during anodization, which disturbs stable growth of the oxide layer.[26] Fortunately, a discontinuous structure is desirous because it can alleviate electrode pulverization due to the large volume expansion that results from nanochannels filling with conductive soft materials during battery cycle testing. As the electrochemically deposited Sn layer is over-etched to reach the Cu substrate, the current density is gradually reduced, exfoliating the oxide layer from the substrate (Step III).

The effect of applied potential and time during the anodization of Sn on Cu foil are shown in Figure 1(c)–(k), demonstrating that the nanochannel pore size increases as a function of

voltage (from 5–10 V) and time (from 10–20 min). In particular, more uniform porous structures were formed at higher voltages. However, an applied voltage above 10 V and time more than 20 min caused the SnO_2 film to peel off from the substrate owing to heavy oxygen evolution and complete consumption of the electrodeposited Sn metal layer (Figure S2).[27] The surface area of anodized samples prepared under diverse conditions was investigated using electrochemical active surface area (ECSA) evaluation, as shown in Figure S3. The ECSA was estimated using a potential range of 0.6–0.9 V (vs. RHE) with scan rates ranging from 0 to 100 mV s^{-1} without Faradaic currents. Samples prepared at 10 V have higher surface areas (219.69 μF cm^2) than those prepared at 5 V (32.04 μF cm^{-2}) and 7 V (53.29 μF cm^{-2}), indicating that surface area increases with increasing anodizing potential. Based on these results, the optimized anodization conditions were determined to be 10 V and 15 min. In agreement with a previous report[10], the anodized layers (which changed color from white to black) are highly flexible, and do not crack or detach from the Cu substrate. This flexibility results from the formation of an amorphous SnO_2 layer onto the Cu substrate, firmly gluing it in place (Figure S4). Therefore, anodized SnO_2 has promising potential in future applications of LIBs with flexible electrodes.[14]

Figure 2(a) shows the XRD patterns of electrochemically deposited Sn metal and anodized SnO_2. The peaks at $2\theta = 30.6°$, 32.0°, 43.8°, and 44.9° are attributed to Sn metal and the rest at $2\theta = 43.3°$, 50.4°, and 74.1° to the Cu substrate (black line). After anodization, no SnO_2 peaks were observed, and only the peaks for Sn and Cu (red line) were present. In addition, XPS analysis was carried out to investigate the elemental composition and chemical bonding in the samples. The Sn 3d spectrum of electrodeposited Sn (bottom of Figure 2(b)) shows three major states, corresponding to metallic Sn (Sn^0), stannous oxide (SnO, Sn^{2+}), and stannic oxide (SnO_2,

Sn^{4+}), which are formed by the highly spontaneous oxidation reaction of the electrodeposited metallic Sn itself.[28, 29] However, for anodic SnO$_2$ (top of Figure 2(b)), only two strong peaks were observed at 487.3 and 495.8 eV, attributed to stannic oxide. The existence of Sn^{4+} confirms that SnO$_2$ was formed. [30] In addition, the XPS spectrum in the O 1s region for anodic SnO$_2$ (Figure 3(c)) shows the expected SnO$_2$ peaks at 530.9, 532.1, and 533.0 eV. The peaks at 530.9 and 532.1 eV are associated with O^{2-} ions in the SnO$_2$ lattice (O$_L$) and oxygen vacancy defects (O$_V$), respectively. The peak at 533.0 eV is attributed to chemisorbed and dissociated oxygen species on the surface (O$_S$).[31, 32] The XRD and XPS results indicate that anodic porous SnO$_2$ layer was amorphous.

CV was used to study electropolymerization of PANI (from suspensions of aniline) onto anodic SnO$_2$ electrodes. Data was recorded in the potential region from −0.5 to 1.5 V (vs. Ag/AgCl) for three cycles with scan rates ranging from 60 to 120 mV s^{-1} (Figure S5). The anodic peak at approximately 0.72 V originates from the polymerization of aniline. This peak's intensity increases as a function of the cycle number, indicating that the amount of PANI deposited onto the electrode increases with more cycles.[33] The SEM images of SnO$_2$@PANI prepared at scan rates of 60, 80, 100, and 120 mV s^{-1} (denoted as SnO$_2$@PANI–60, 80, 100, and 120, respectively) are shown in Figure 3(a)–(d), and verify that the porous structure of the SnO$_2$ coating is maintained after electrodeposition of polyaniline. However, lower scan rates led to the formation of thicker PANI layers, causing a decrease in the pore size of the SnO$_2$@PANI anodes: the pore size of SnO$_2$@PANI–60 is the smallest, while the pore size of SnO$_2$@PANI–120 is almost identical to that of the uncoated SnO$_2$@PANI electrode. The TEM images of SnO$_2$@PANI–100 (Figure 3(e) and 3(f)) confirm that the porous structure of SnO$_2$ remains intact and is uniformly coated with a polymerized layer of PANI with a thickness of

approximately 3 nm. Furthermore, the TEM–EDS mapping analysis (Figure 3(g)) indicates that the distribution of Sn, O, C, and N throughout the composite is uniform.

The existence of electropolymerized PANI is confirmed by the FT–IR spectra of SnO_2@PANI anodes (Figure 4(a)). The spectra exhibit characteristic bands due to PANI at 1593, 1503, 1305, 1155, and 827 cm^{-1}, proving that the CV approach successively electropolymerized PANI onto porous SnO_2 structures. Among these characteristic bands of SnO_2@PANI, those at 1593 and 1503 cm^{-1} are attributed to the C=C stretch of the quinonoid and benzenoid rings, respectively. The peak at 1305 cm^{-1} corresponds to the C–N stretch of the secondary aromatic amine and that at 1155 cm^{-1} corresponds to the aromatic C–H in-plane bending. The peak at 827 cm^{-1} is associated with the out-of-plane deformation of C–H in the 1,4-disubstituted benzene ring.[34]

The successful formation of PANI onto the porous SnO_2 electrode was further confirmed by the XPS spectra of SnO_2 and SnO_2@PANI, as shown in Figure 4(b), where peaks due to C 1s and N 1s spectra appear only after electropolymerization. The high-resolution C 1s spectrum (Figure 4(c)) can be peak-fitted at 284.9 eV, 286.1 eV, and 288.0 eV, which are attributed to the C–C/C–H, C–N, and C–O bonds, respectively. The four peaks in Figure 4(d) indicate that the N 1s spectrum is in the form of benzenoid amine (–NH–) with a binding energy centered at 399.8 eV and quinoid imine (–N=) at 398.8 eV. Positively charged nitrogen cationic radicals (N$^+$) are centered at 400.6 eV and 401.8 eV.[35, 36]

3.2. Electrochemical analysis

The anode performance of SnO_2 and SnO_2@PANI in lithium half-cells were evaluated to investigate the effect of the applied voltage during anodization and the thickness of the PANI layer on the anodic SnO_2 electrode. The cycling performance of the SnO_2 electrode grown

directly on the Cu substrate was measured at a current density of 0.1 A g^{-1}. As shown in Figure S6, the nanoporous SnO_2 prepared at a higher applied anodization potential exhibits a higher discharge capacity than those prepared at lower applied potentials. This is owing to the resulting larger electrochemical surface area where Li$^+$ ions can be stored. However, after the 50th cycle, the capacity retention of the SnO_2 electrode prepared with an applied potential of 10 V was only 28.82% compared with that after the 5th cycle. This indicates that the introduction of a buffer layer to suppress volume expansion is necessary. Figure 5(a) shows the initial four CV curves of the SnO_2@PANI electrode obtained at a scan rate of 0.1 mV s^{-1} over the potential range of 0.01–3.0 V (vs. Li/Li$^+$). During the first cathode scan, the reduction peak at ~0.9 V is associated with the formation of solid electrolyte interphase (SEI), accompanied with the irreversible reduction of SnO_2 to metallic Sn.[14,37, 38] The reduction peak at ~0.1 V and the oxidation peak at ~0.6 V correspond to the two-step Li-Sn alloying/dealloying process of the Li-Sn alloy (Equations 1 and 2) that predominantly contributes to the overall capacity.[39] In the following cycles, the reduction peak at 0.1 V shifts to a higher potential of 0.31 V due to the formation of intermediate products of Li-Sn alloy during the multi-step alloying process.[10] The other redox peak pairs at potentials of 0.58 V, 1.25 V and 1.20 V, 1.78 V are attributed to the partially reversible reactions of Sn to SnO and SnO_2.[40, 41] The CV curves after the first cycle almost overlap, showing good cycling reversibility of SnO_2@PANI electrode. There is no apparent peak corresponding to PANI in the CV curve, implying that the PANI coating does not contribute to the capacity of the overall lithium alloying/dealloying reactions.

$$SnO_2 + 4Li^+ + 4e^- \rightarrow Sn + 2Li_2O$$

(1)

$$Sn + xLi^+ + xe^- \rightarrow Li_xSn \ (0 \leq x \leq 4.4)$$
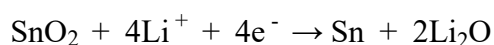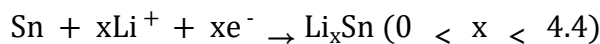
(2)

Figure 5(b) shows the charge/discharge profiles of SnO_2@PANI–100 for selective cycles at a current density of 0.1 A g^{-1}. The initial capacity loss from the discharge capacity of 1644 to 1002 mA h g^{-1} is mainly attributed to the irreversible reduction of SnO_2 to metallic Sn and electrolyte decomposition caused by the formation of an SEI layer. As the cycle progresses, the plateau at 1.2 V disappears, meaning that the reduction reaction of SnO_2 to metallic Sn (Equation 1) is irreversible. It exhibits a specific capacity of ~440 mA h g^{-1} after 50 cycles at a current density of 0.1 A g^{-1}, which is comparable to the other SnO2@PANI-based electrodes (Table S1). The cycling performance of the SnO_2@PANI anodes prepared at scan rates ranging from 60 to 120 mV s^{-1} was tested at a current density of 0.1 A g^{-1}. As shown in Figure 5(c), despite the increase in the total mass due to the addition of PANI onto the porous SnO_2 electrode, the capacity after 50 cycles is clearly greater than that of the uncoated nanoporous SnO_2 electrode. This is attributed to the larger lithium diffusion coefficient of PANI than SnO_2, favoring the lithium diffusion process.[42, 43] An increased capacity retention, ranging from 45.34 to 52.63%, after 50 cycles compared with five cycles was measured. Figure 5(d) shows that capacity retention increases when the scan rate is increased from 60 to 100 mV s^{-1}, but then decreases when the scan rate is increased to 120 mV s^{-1}. These results demonstrate that the SnO_2@PANI–100 electrode effectively reduces SnO_2 volume expansion, while maintaining pores of sufficient size to allow for the diffusion of lithium ions into the nanoporous SnO_2 structures. Figure 5(e) shows the rate performance of the uncoated nanoporous SnO_2 and SnO_2@PANI–100 electrode at different current densities. The specific capacities of the SnO_2@PANI–100 electrode at all current densities were higher than that of the uncoated SnO_2,

indicating that the rate capability of the SnO_2@PANI–100 electrode is better than that of SnO_2 owing to the PANI buffer layer.

EIS measurements were conducted to further investigate the charge-transfer kinetics at the interface between the electrode and electrolyte. The Nyquist plots of SnO_2 and the SnO_2@PANI electrodes after 50 cycles at a current density of 0.1 A g^{-1} are shown in Figure 6. From the inset of the equivalent electrical circuit, the semicircles in the high- and mid-frequency regions are attributed to the resistance to SEI formation (R_{sf}) and charge transfer resistance at the interface between the electrode and electrolyte (R_{ct}), respectively. The straight line at low frequency is related to the Warburg impedance of lithium ion diffusion. As summarized in Table 1, owing to the conductive properties of PANI the SnO_2@PANI electrodes exhibit much lower charge transfer resistance compared with the uncoated nanoporous SnO_2 electrode. The lowest charge transfer resistance was recorded using SnO_2@PANI–100 (20.69 Ω), resulting in the facile transfer of lithium ions and electrons at the interface between this electrode and the electrolyte. In addition, in the low-frequency region, the straight line graph of imaginary impedance against real impedance has a steeper slope for the SnO_2@PANI electrodes than for the uncoated SnO_2 electrode, indicating faster Li ion diffusion, which is consistent with the cycling performance observed in Figure 5(c).[44]

4. Conclusions

In summary, SnO_2@PANI anodes were successfully synthesized through the electrochemical deposition of Sn onto a Cu substrate, anodization of Sn, and the electropolymerization of PANI as a buffer layer to reduce volume expansion and improve diffusion kinetics of Li^+ ions during battery charging and discharging. The anodic SnO_2 binder-free anode grown directly onto a Cu substrate has 3D nanoporous structures with a large surface area, high porosity, and excellent structural flexibility with good adhesion on Cu foil. This leads to shortened lithium ion diffusion lengths and improved electron transport, resulting in improved electrochemical properties. In addition, uniformly deposited PANI onto nanoporous SnO_2 electrodes serves as an effective buffer layer. Optimizing the thickness of PANI by controlling the scan rate offered a high electrical conductivity and relieved the severe volume expansion caused by lithiation of the SnO_2 electrode. The SnO_2@PANI–100 electrode exhibits a specific capacity of ~440 mA h g^{-1} after 50 cycles at a current density of 0.1 A g^{-1}, with a low charge transfer resistance and high lithium diffusion kinetics. We believe that the proposed fabrication process is a potentially cost–effective, simple, and easily scalable approach for designing SnO_2@PANI binder-free electrodes with high performance in flexible LIBs.

Appendix A. Supplementary data

Supplementary data related to this article can be found at online.

Acknowledgement

Conflict of interest:

The authors declare no conflicts of interest.

References

1.   Nishi, Y., Lithium ion secondary batteries; past 10 years and the future. *Journal of Power Sources* **2001,** *100* (1-2), 101-106.

2.   Kang, B.; Ceder, G., Battery materials for ultrafast charging and discharging. *Nature* **2009,** *458* (7235), 190-193.

3.   Cabana, J.;   Monconduit, L.;   Larcher, D.; Palacin, M. R., Beyond intercalation-based Li-ion batteries: the state of the art and challenges of electrode materials reacting through conversion reactions. *Advanced materials* **2010,** *22* (35), E170-E192.

4.   Chen, J. S.; Lou, X. W., SnO2-based nanomaterials: synthesis and application in lithium-ion batteries. *small* **2013,** *9* (11), 1877-1893.

5.   Zhao, Q.;   Ma, L.;   Zhang, Q.;   Wang, C.; Xu, X., SnO2-based nanomaterials: synthesis and application in lithium-ion batteries and supercapacitors. *journal of Nanomaterials* **2015,** *2015*.

6.   Li, Q.;   Li, H.;   Xia, Q.;   Hu, Z.;   Zhu, Y.;   Yan, S.;   Ge, C.;   Zhang, Q.; Wang, X.; Shang, X., Extra storage capacity in transition metal oxide lithium-ion batteries revealed by in situ magnetometry. *Nature materials* **2021,** *20* (1), 76-83.

7.   Hu, C.;   Chen, L.;   Hu, Y.;   Chen, A.;   Chen, L.;   Jiang, H.; Li, C., Light-Motivated SnO2/TiO2 Heterojunctions Enabling the Breakthrough in Energy Density for Lithium-Ion Batteries. *Advanced Materials* **2021,** *33* (49), 2103558.

8.   Huang, J. Y.;   Zhong, L.;   Wang, C. M.;   Sullivan, J. P.;   Xu, W.;   Zhang, L. Q.; Mao, S. X.;   Hudak, N. S.;   Liu, X. H.; Subramanian, A., In situ observation of the electrochemical lithiation of a single SnO2 nanowire electrode. *Science* **2010,** *330* (6010), 1515-1520.

9.   Yesibolati, N.;   Shahid, M.;   Chen, W.;   Hedhili, M. N.;   Reuter, M. C.;   Ross, F. M.; Alshareef, H. N., SnO2 Anode Surface Passivation by Atomic Layer Deposited HfO2 Improves Li-Ion Battery Performance. *Small* **2014,** *10* (14), 2849-2858.

10.   Liu, J.; Xie, D.; Xu, X.; Jiang, L.; Si, R.;   Shi, W.; Cheng, P., Reversible formation of coordination bonds in Sn-based metal-organic frameworks for high-performance lithium storage. *Nature communications* **2021,** *12* (1), 1-10.

11.   Etacheri, V.; Seisenbaeva, G. A.; Caruthers, J.; Daniel, G.; Nedelec, J. M.; Kessler, V. G.; Pol, V. G., Ordered network of interconnected SnO2 nanoparticles for excellent lithium-ion storage. *Advanced Energy Materials* **2015,** *5* (5), 1401289.

12.   Wang, H.; Rogach, A. L., Hierarchical SnO2 nanostructures: recent advances in design, synthesis, and applications. *Chemistry of Materials* **2014,** *26* (1), 123-133.

13.   Li, H.; Hu, Z.; Xia, Q.; Zhang, H.; Li, Z.; Wang, H.; Li, X.; Zuo, F.; Zhang, F.; Wang, X., Operando magnetometry probing the charge storage mechanism of CoO lithium-ion batteries. *Advanced Materials* **2021,** *33* (12), 2006629.

14.   Zhang, F.; Teng, X.; Shi, W.; Song, Y.; Zhang, J.; Wang, X.; Li, H.; Li, Q.; Li, S.; Hu, H., SnO2 nanoflower arrays on an amorphous buffer layer as binder-free electrodes for flexible lithium-ion batteries. *Applied Surface Science* **2020,** *527*, 146910.

15.   Song, D.; Wang, S.; Liu, R.; Jiang, J.; Jiang, Y.; Huang, S.; Li, W.; Chen, Z.; Zhao, B., Ultra-small SnO2 nanoparticles decorated on three-dimensional nitrogen-doped graphene aerogel for high-performance bind-free anode material. *Applied Surface Science* **2019,** *478*, 290-298.

16.   Hu, Y.; Ye, D.; Luo, B.; Hu, H.; Zhu, X.; Wang, S.; Li, L.; Peng, S.; Wang, L., A binder-free and free-standing cobalt sulfide@ carbon nanotube cathode material for aluminum-ion batteries. *Advanced Materials* **2018,** *30* (2), 1703824.

17.   Prakasam, H. E.; Shankar, K.; Paulose, M.; Varghese, O. K.; Grimes, C. A., A new benchmark for TiO2 nanotube array growth by anodization. *The Journal of Physical Chemistry C* **2007,** *111* (20), 7235-7241.

18.   Piao, Y.; Kim, H., Fabrication of nanostructured materials using porous alumina template and their applications for sensing and electrocatalysis. *Journal of Nanoscience and Nanotechnology* **2009,** *9* (4), 2215-2233.

19.   Wu, Q.; Xu, Y.; Yao, Z.; Liu, A.; Shi, G., Supercapacitors based on flexible graphene/polyaniline nanofiber composite films. *ACS nano* **2010,** *4* (4), 1963-1970.

20.   Zhang, X.; Ji, L.; Zhang, S.; Yang, W., Synthesis of a novel polyaniline-intercalated layered manganese oxide nanocomposite as electrode material for electrochemical capacitor. *Journal of Power Sources* **2007,** *173* (2), 1017-1023.

21.   Sun, X.; Zhang, Y.; Zhang, J.; Zaman, F. U.; Hou, L.; Yuan, C., Bi-Metal (Zn, Mn) Metal–Organic Framework–Derived ZnMnO3 Micro-Sheets Wrapped Uniformly with

Polypyrrole Conductive Network toward High-Performance Li-Ion Batteries. *Energy Technology* **2020,** *8* (3), 1901218.

22.   Pimphor, K.; Roddecha, S., The optimization and comparison of the electrochemical performances for the polyaniline and melamine doping onto activated porous carbon material derived from pineapple leaf fiber as anode material for lithium-ion batteries. *Materials Today: Proceedings* **2021,** *47*, 3610-3616.

23.   Shi, M.; Liu, Z.; Zhang, S.; Liang, S.; Jiang, Y.; Bai, H.; Jiang, Z.; Chang, J.; Feng, J.; Chen, W., A Mott–Schottky Heterogeneous Layer for Li–S Batteries: Enabling Both High Stability and Commercial-Sulfur Utilization. *Advanced Energy Materials*, 2103657.

24.   Heubner, C.; Liebmann, T.; Voigt, K.; Weiser, M.; Matthey, B. r.; Junker, N.; Lämmel, C.; Schneider, M.; Michaelis, A., Scalable fabrication of nanostructured tin oxide anodes for high-energy lithium-ion batteries. *ACS applied materials & interfaces* **2018,** *10* (32), 27019-27029.

25.   Asseli, R.; Benaicha, M.; Derbal, S.; Allam, M.; Dilmi, O., Electrochemical nucleation and growth of Zn-Ni alloys from chloride citrate-based electrolyte. *Journal of Electroanalytical Chemistry* **2019,** *847*, 113261.

26.   Zaraska, L.; Czopik, N.; Bobruk, M.; Sulka, G. D.; Mech, J.; Jaskuła, M., Synthesis of nanoporous tin oxide layers by electrochemical anodization. *Electrochimica Acta* **2013,** *104*, 549-557.

27.   Cao, J.; Gao, Z.; Wang, C.; Muzammal, H. M.; Wang, W.; Gu, Q.; Dong, C.; Ma, H.; Wang, Y., Morphology evolution of the anodized tin oxide film during early formation stages at relatively high constant potential. *Surface and Coatings Technology* **2020,** *388*, 125592.

28.   Won, D. H.; Choi, C. H.; Chung, J.; Chung, M. W.; Kim, E.-H.; Woo, S. I., Rational Design of a Hierarchical Tin Dendrite Electrode for Efficient Electrochemical Reduction of CO2. *ChemSusChem* **2015,** *8* (18), 3092-3098.

29.   Yang, Y.; Liu, J.; Li, C.; Fu, L.; Huang, W.; Li, Z., Fabrication of pompon-like and flower-like SnO microspheres comprised of layered nanoflakes by anodic electrocrystallization. *Electrochimica acta* **2012,** *72*, 94-100.

30.   Hong, Y.; Mao, W.; Hu, Q.; Chang, S.; Li, D.; Zhang, J.; Liu, G.; Ai, G., Nitrogen-doped carbon coated SnO2 nanoparticles embedded in a hierarchical porous carbon

framework for high-performance lithium-ion battery anodes. *Journal of Power Sources* **2019,** *428*, 44-52.

31.   Motsoeneng, R. G.;   Kortidis, I.;   Ray, S. S.; Motaung, D. E., Designing SnO2 nanostructure-based sensors with tailored selectivity toward propanol and ethanol vapors. *ACS omega* **2019,** *4* (9), 13696-13709.

32.   Supothina, S.; De Guire, M. R., Characterization of SnO2 thin films grown from aqueous solutions. *Thin Solid Films* **2000,** *371* (1), 1-9.

33.   Nasr-Esfahani, P.;   Ensafi, A. A.; Rezaei, B., Fabrication of a highly sensitive and selective modified electrode for imidacloprid determination based on designed nanocomposite graphene quantum dots/ionic liquid/multiwall carbon nanotubes/polyaniline. *Sensors and Actuators B: Chemical* **2019,** *296*, 126682.

34.   Chen, S.;   Wei, Z.;   Qi, X.;   Dong, L.;   Guo, Y.-G.;   Wan, L.;   Shao, Z.; Li, L., Nanostructured Polyaniline-Decorated Pt/C@PANI Core–Shell Catalyst with Enhanced Durability and Activity. *Journal of the American Chemical Society* **2012,** *134* (32), 13252-13255.

35.   Gao, Z.;   Yang, W.;   Wang, J.;   Yan, H.;   Yao, Y.;   Ma, J.;   Wang, B.;   Zhang, M.;   Liu, L., Electrochemical synthesis of layer-by-layer reduced graphene oxide sheets/polyaniline nanofibers composite and its electrochemical performance. *Electrochimica Acta* **2013,** *91*, 185-194.

36.   Zhang, J.;   Xu, Y.;   Fan, L.;   Zhu, Y.;   Liang, J.; Qian, Y., Graphene–encapsulated selenium/polyaniline core–shell nanowires with enhanced electrochemical performance for Li–Se batteries. *Nano Energy* **2015,** *13*, 592-600.

37.   Di Lupo, F.;   Gerbaldi, C.;   Meligrana, G.;   Bodoardo, S.; Penazzi, N., Novel SnO2/mesoporous carbon spheres composite anode for Li-ion batteries. *Int. J. Electrochem. Sci* **2011,** *6*, 3580-3593.

38.   Sun, X.;   Liu, Y.;   Zhang, J.;   Hou, L.;   Sun, J.; Yuan, C., Facile construction of ultrathin SnOx nanosheets decorated MXene (Ti3C2) nanocomposite towards Li-ion batteries as high performance anode materials. *Electrochimica Acta* **2019,** *295*, 237-245.

39.   Wen, Z.;   Wang, Q.;   Zhang, Q.; Li, J., In situ growth of mesoporous SnO2 on multiwalled carbon nanotubes: A novel composite with porous-tube structure as anode for lithium batteries. *Advanced Functional Materials* **2007,** *17* (15), 2772-2778.

40.   Huang, M.; Feng, M.; Li, H.; Huang, P.; Su, Q.; Zhang, F.; Du, G., Rapid microwave-assisted synthesis of SnO2 quantum dots/reduced graphene oxide composite with its application in lithium-ion battery. *Materials Letters* **2017,** *209*, 260-263.

41.   Shao, Q.; Tang, J.; Sun, Y.; Li, J.; Zhang, K.; Yuan, J.; Zhu, D.-M.; Qin, L.-C., Unique interconnected graphene/SnO 2 nanoparticle spherical multilayers for lithium-ion battery applications. *Nanoscale* **2017,** *9* (13), 4439-4444.

42.   Zhang, F.; Yang, C.; Gao, X.; Chen, S.; Hu, Y.; Guan, H.; Ma, Y.; Zhang, J.; Zhou, H.; Qi, L., SnO2@ PANI core–shell nanorod arrays on 3D graphite foam: a high-performance integrated electrode for lithium-ion batteries. *ACS applied materials & interfaces* **2017,** *9* (11), 9620-9629.

43.   Hou, L.; Bao, R.; kionga Denis, D.; Sun, X.; Zhang, J.; uz Zaman, F.; Yuan, C., Synthesis of ultralong ZnFe2O4@ polypyrrole nanowires with enhanced electrochemical Li-storage behaviors for lithium-ion batteries. *Electrochimica Acta* **2019,** *306*, 198-208.

44.   Jeong, J. M.; Choi, B. G.; Lee, S. C.; Lee, K. G.; Chang, S. J.; Han, Y. K.; Lee, Y. B.; Lee, H. U.; Kwon, S.; Lee, G., Hierarchical hollow spheres of Fe2O3@ polyaniline for lithium ion battery anodes. *Advanced Materials* **2013,** *25* (43), 6250-6255.
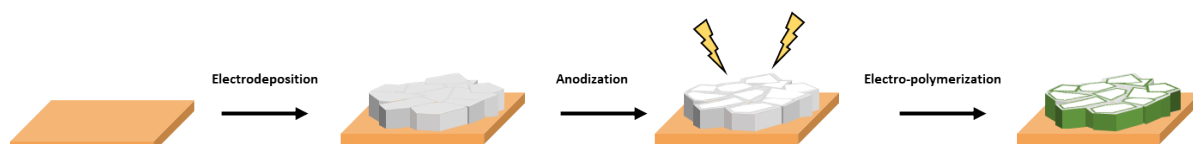
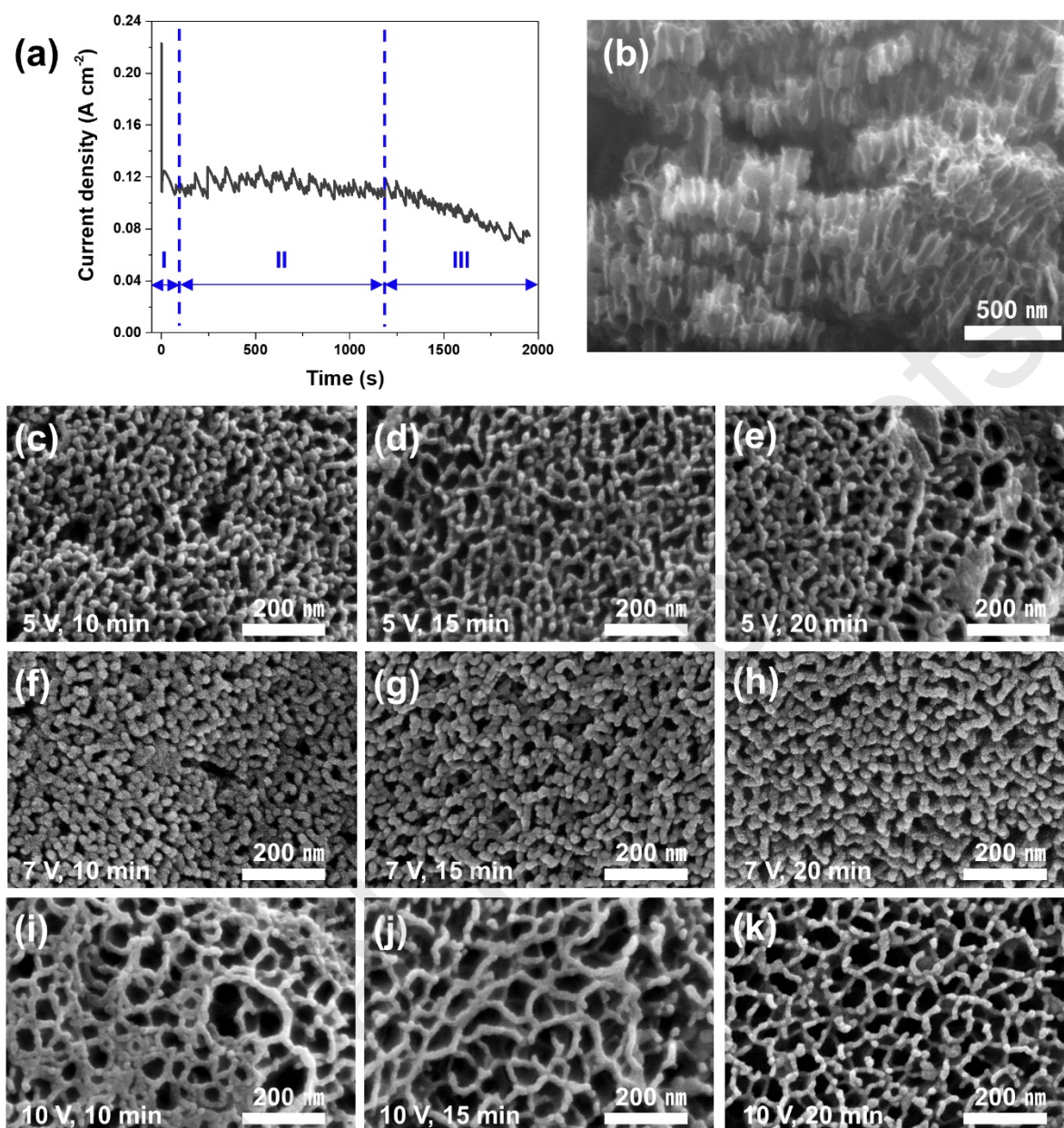**Scheme 1.** Illustration of the SnO$_2$@PANI electrode fabrication process.

Figure 1. (a) I-t curve of electrodeposited Sn anodization. SEM images of (b) SnO_2 nanochannels and (c-k) porous surfaces of SnO_2 fabricated by anodization using different voltages and times.
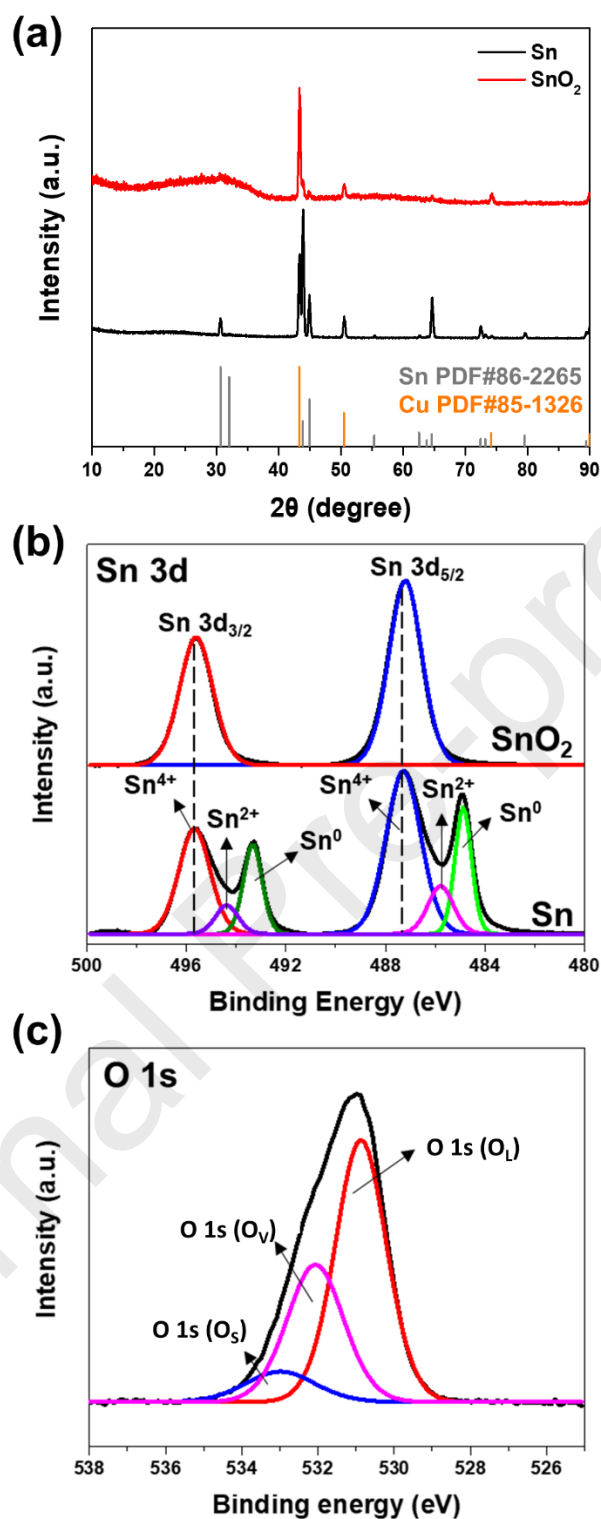
22

Figure 2. (a) XRD of electrodeposited Sn and anodized SnO$_2$. The (b) Sn 3d XPS spectrum of electrodeposited Sn (bottom) and anodized SnO$_2$ (top) and (c) O 1s XPS spectrum of SnO$_2$.
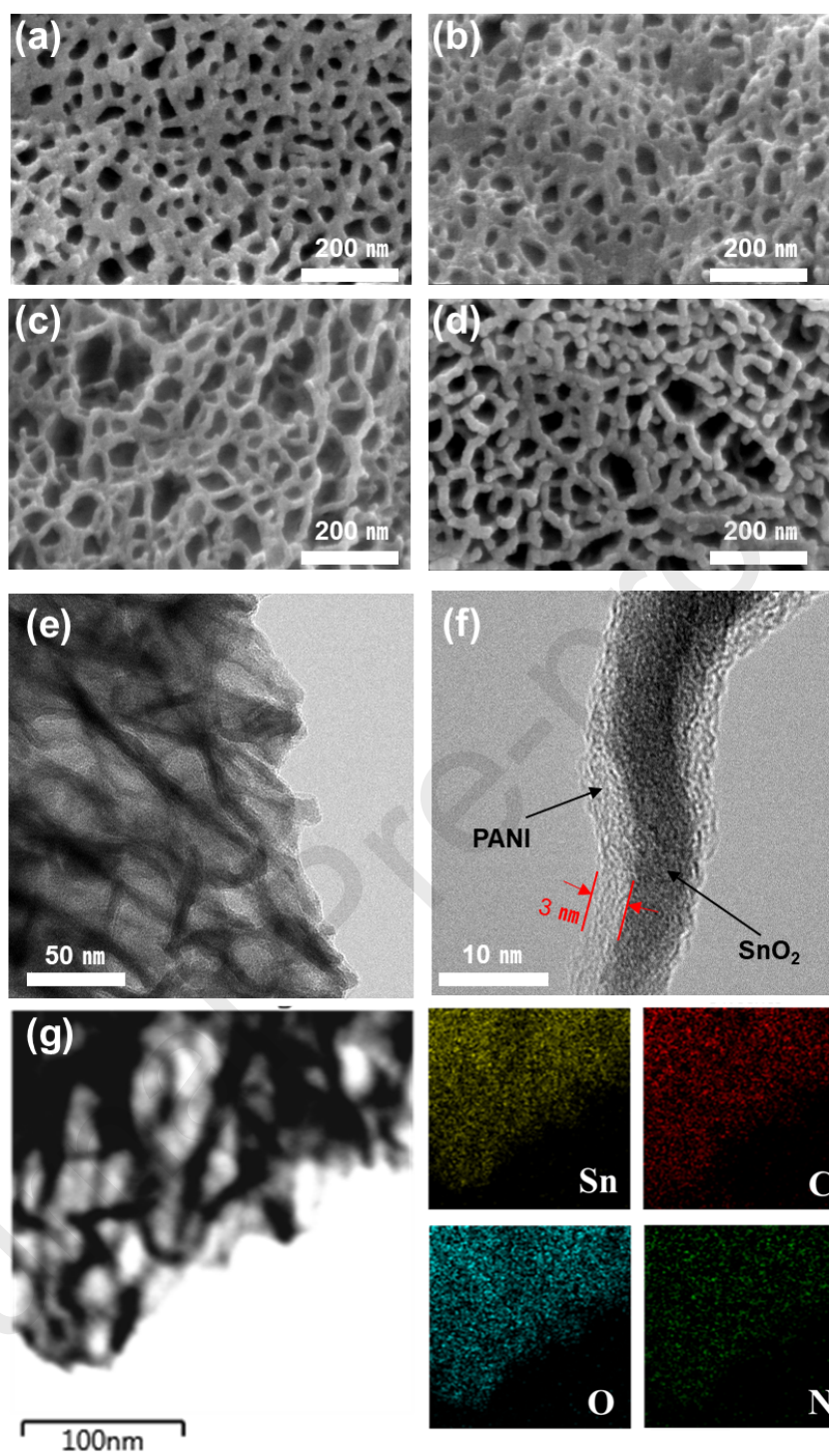
Figure 3. SEM images of aniline electropolymerized on SnO$_2$ at cyclic voltammetry scan rates of (a) 60 mV s^{-1}, (b) 80 mV s^{-1}, (c) 100 mV s^{-1}, (d) 120 mV s^{-1}. SnO$_2$@PANI-100 (e), (f) TEM images and (g) EDS-mapping.
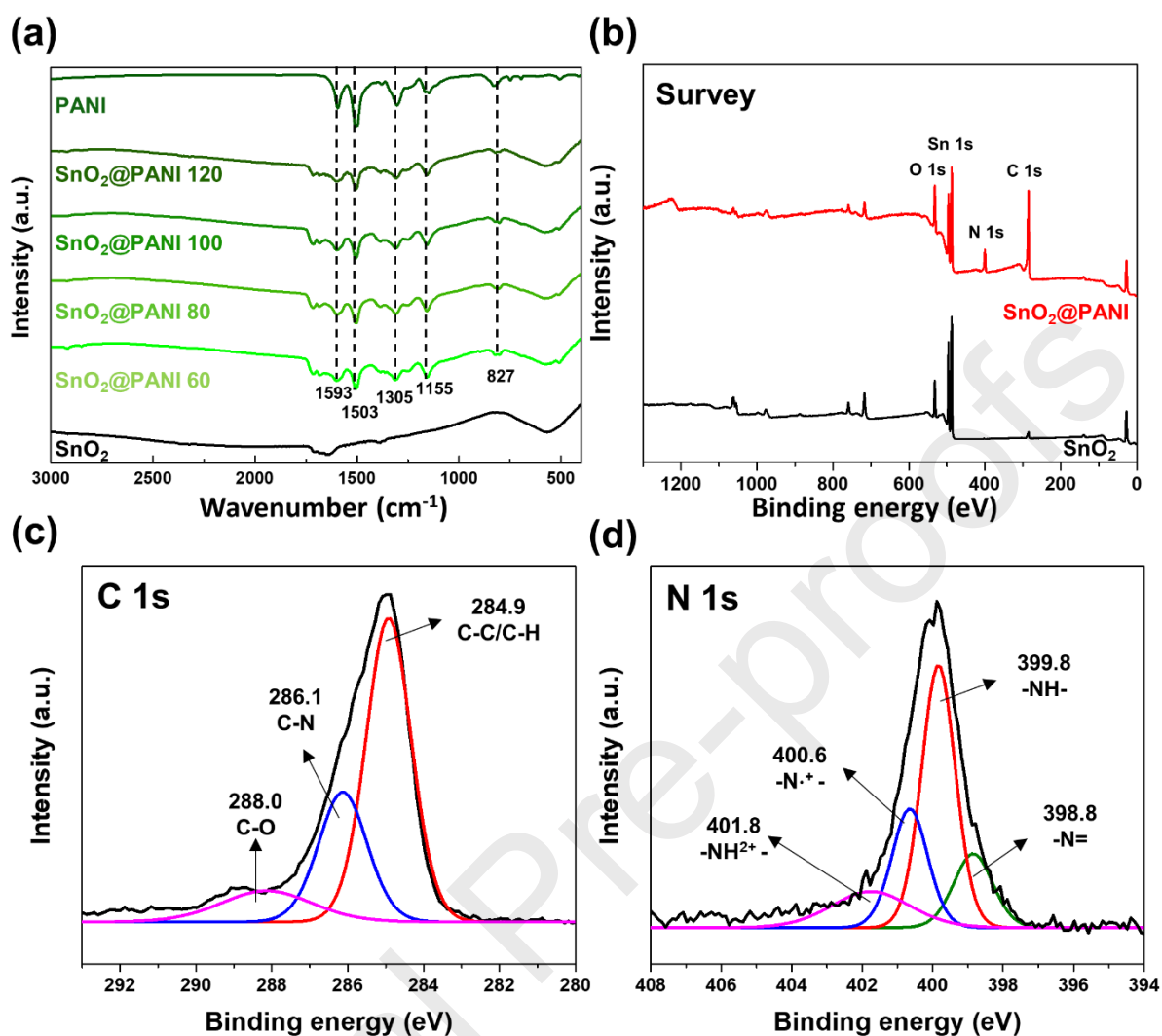
Figure 4. (a) FT-IR spectra of SnO_2 and $SnO_2@PANI$ at various electropolymerization cyclic voltammetry scan rates. (b) XPS survey spectra of SnO_2 and $SnO_2@PANI$. High-resolution XPS spectra of (c) C 1s and (d) N 1s for $SnO_2@PANI$.
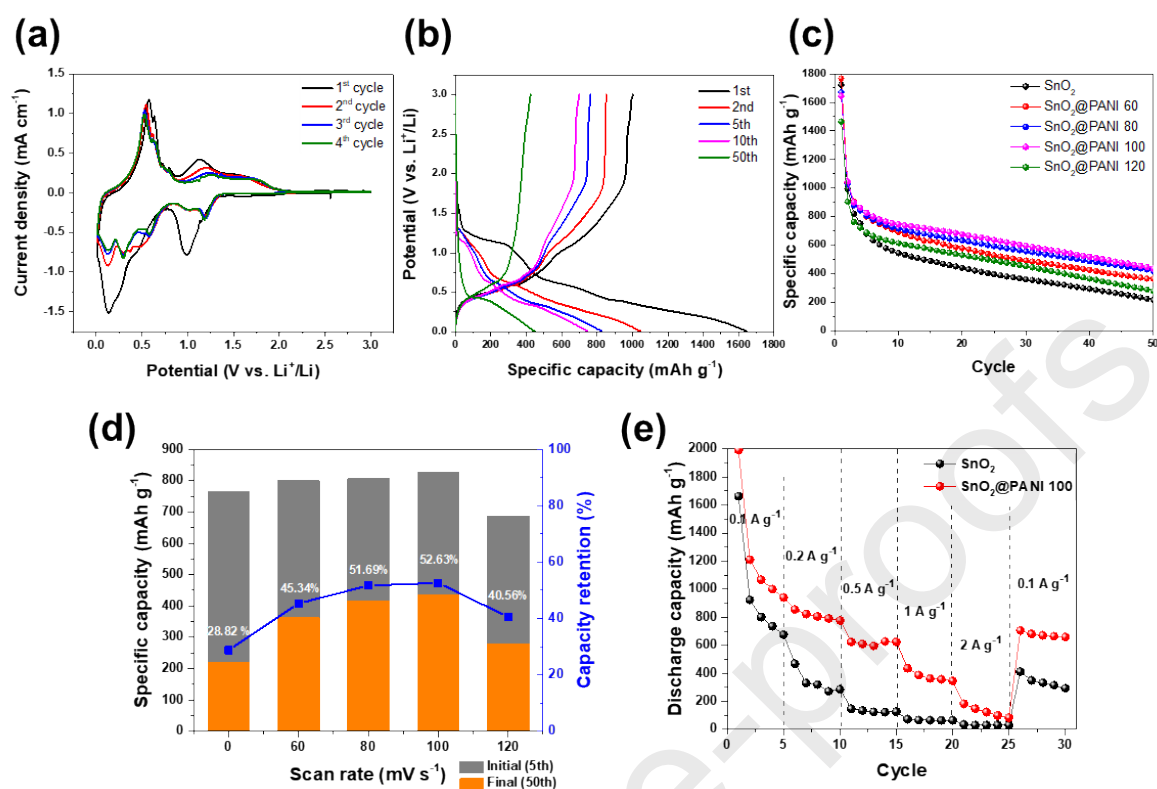
Figure 5. Electrochemical performance of SnO_2@PANI 100: (a) Cyclic voltammetry, (b) galvanostatic charge/discharge profiles. (c) Cycling performance of SnO_2 and various SnO_2@PANI electrodes at a current density of 100 mA g^{-1}. (d) Diagram of SnO_2@PANI 100 specific capacity and capacity retention after 50 cycles, (e) rate capability at different discharge current densities of SnO_2@PANI 100 compared with SnO_2.
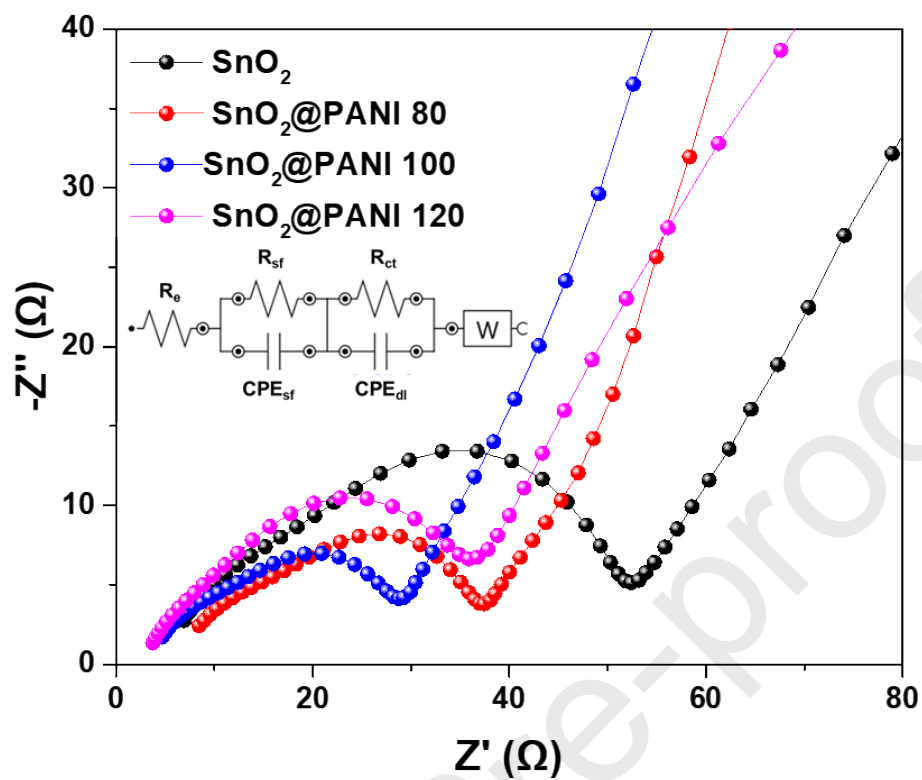
Figure 6. Electrochemical impedance spectra of SnO_2, SnO_2@PANI 80, SnO_2@PANI 100, and SnO_2@PANI 120.

Table 1. Impedance parameters for SnO_2, SnO_2@PANI 80, SnO_2@PANI 100, and SnO_2@PANI 120 after 50 cycles as measured by an equivalent electric circuit.

Materials	R_e [Ω]	R_{sf} [Ω]	R_{ct} [Ω]
SnO_2	6.91	23.53	40.20
SnO_2@PANI 80	8.44	15.40	25.17
SnO_2@PANI 100	4.66	14.85	20.69
SnO_2@PANI 120	3.75	16.65	32.57

CRediT author statement

Nahyun Shin: Conceptualization, Investigation, Data curation, Visualization, Writing – Original draft. **Moonsu Kim:** Formal analysis, Investigation. **Jaeyun Ha:** Formal analysis, Investigation. **Yong-Tae Kim:** Conceptualization, Visualization, Writing – review & editing, Supervision. **Jinsub Choi:** Conceptualization, Writing – review & editing, Supervision, Funding acquisition.

Declaration of interests

☒ The authors declare that they have no known competing financial interests or personal relationships that could have appeared to influence the work reported in this paper.

☐ The authors declare the following financial interests/personal relationships which may be considered as potential competing interests:

Highlights

- SnO_2@PANI anodes were successfully synthesized through wet-chemical approach.

- Anodic nanoporous SnO_2 leads to shortened lithium ion diffusion lengths.

- Uniformly deposited PANI onto nanoporous SnO_2 serves as an effective buffer layer.

- Optimized thickness of PANI layer is controlled by adjusting the scan rate.